Weather and Climate Extremes 5-6 (2014) 56–66

Contents lists available at ScienceDirect

Weather and Climate Extremes

journal homepage: www.elsevier.com/locate/wace

Future changes in extreme temperature events using the statistical downscaling model (SDSM) in the trans-boundary region of the Jhelum river basin

Rashid Mahmood [a,*], Mukand S Babel [b]

[a] Department of Irrigation and Drainage, Faculty of Agricultural Engineering and Technology, University of Agriculture, Faisalabad, Pakistan
[b] Department of Water Engineering and Management, School of Engineering and Technology, Asian Institute of Technology, Pathumthani, Thailand

ARTICLE INFO

Article history:
Received 1 April 2014
Received in revised form
15 July 2014
Accepted 12 September 2014
Available online 22 September 2014

Keywords:
Climate change
Frequency indices
Intensity indices
Downscaling
Pakistan
India

ABSTRACT

In the 21st century, climate change is considered to be one of the greatest environmental threats to the world, and the changes in climate extremes are estimated to have greater negative impacts on human society and the natural environment than the changes in mean climate. This study presents the projections of future changes in extreme temperature events under A2 and B2 SRES scenarios using the statistical downscaling model (SDSM) in the trans-boundary region of the Jhelum River basin. This area is located in Pakistan and India. In order to get realistic results, bias correction was also applied to downscale the daily maximum and minimum temperature values before calculating 8 intensity and 4 frequency indices. Validation (1991–2000) showed great reliability of SDSM in ascertaining changes for the periods 2011–2040, 2041–2070 and 2071–2099, relative to 1961–1990.

The intensity of the highest and the lowest night time temperatures is simulated to be higher than the highest and lowest day time temperatures. In contrast, the intensity of high night time temperature (hot nights) is projected to be lower than high day time temperature (hot days). The number of hot days and hot nights is predicted to increase, and by contrast, the frequency of cold days and cold night is predicted to decrease in all three future periods. Almost all the seasons will witness warming effects in the basin. However, these effects are much more serious in spring (hot days and nights) and in winter (cold and frosty days).

On the whole in the Jhelum basin, the intensity and frequency of warm temperature extremes are likely to be higher and the intensity and frequency of cold temperature extremes to be lower in the future.

1. Introduction

According to the 5th Assessment Report (AR5) of the Intergovernmental Panel on Climate Change (IPCC), global (land and ocean) average temperature has shown a 0.85 °C (0.65–1.06 °C) increase over the period of 1800–2012 (IPCC, 2013), and a 0.74 ± 0.18 °C increase during the last hundred years (1906–2005) (IPCC, 2007). This trend in global warming is predicted to *likely* increase during the 21st century under all the Representative Concentration Pathways (RCPs). The projected values of increase are 0.3–1.7 °C (RCP2.6), 1.1–2.6 °C (RCP4.5), 1.4–3.1 °C (RCP6.0), 2.6–4.8 °C (RCP8.5) for 2081–2100, relative to 1986–2005 (IPCC, 2013). Such changes in globle mean temperature can radically disturb human society and the natural environment (Ashiq et al., 2010). However, the changes in extreme temperature events such as heat waves, severe winter and summer storms, hot and cold days, and hot and cold nights (Mastrandrea et al., 2011) can cause more severe impacts on human society and the natural environment. Consequently, extreme events have got greater attention by scientists in the last few years (Sanchez et al., 2004). It is reported in AR5 that between 1951 and 2010, the number of warm days and nights has increased, and the number of cold days and nights has decreased on a global scale. In addition, the time length and frequency of warm spells, including heat waves, have also increased since the middle of the 20th century (IPCC, 2013).

In the last one decade, many studies have reported different extreme temperature events due to climate change in many regions of the globe; for example, the 2003 summer heat wave over Europe and the Russian heat wave (Zong and Chen, 2000; Schar and Jendritzky, 2004; Cheng et al., 2012; Frias et al., 2012;

* Corresponding author. Tel: +92 41 920 0161.
E-mail address: rashi1254@gmail.com (R. Mahmood).

http://dx.doi.org/10.1016/j.wace.2014.09.001

Lau and Kim, 2012). Huynen et al. (2001) explored how extreme cold or hot temperature events can increase human mortality rates (Huynen et al., 2001).

Changes in extreme events have triggered massive consequences for human society and for the natural environment all over the world. Moreover, climate change has the potential to change the intensity and frequency of extremes. More severe climate changes can cause more severe extreme events, causing dramatic impacts with unpredictable consequences. Therefore, the prediction of climate extremes is critical information that is needed to assess the impact of potential climate change on human beings and on the natural environment. Such information is also vital for long-term planning at regional and national levels for mitigation and adaptation strategies (Frias et al., 2012; Gu et al., 2012).

Currently, a commonly used approach for predicting the variability and changes in climate variables, on global and continental levels, is to drive Global Climate Models (GCMs) with different emission scenarios of CO_2 (Fowler et al., 2007; Gu et al., 2012). However, the GCMs' coarse resolutions (100–500 km) reduce their applicability where regional scales are concerned. Regional scales require a high resolution to adequately represent complex topographical features when the environmental and hydrological impacts of climate change are to be examined there. Topographies such as the Tibet Plateau and the Himalayas in Asia are cases in point (Gu et al., 2012).

To overcome this problem, several statistical and dynamical downscaling models have been developed in the last two decades to make the GCMs' coarse temporal and spatial outputs useful at a local or regional level (Mahmood and Babel, 2013). The local scale is defined as 0–50 km and the regional scale as 50×50 km (Xu, 1999). Among these downscaling models, the Statistical Downscaling Model (SDSM) has been used widely throughout the world in climate change (both mean and extreme) assessment studies (Wilby et al., 2002; Gachon et al., 2005; Gagnon et al., 2005; Chu et al., 2010; Huang et al., 2011; Wang et al., 2012; Mahmood and Babel, 2013).

A few studies carried out in East and South Asia, such as Islam et al. (2009), Gu et al. (2012), Revadekar et al. (2012) and Wang et al. (2012), explore observed and future changes in extreme temperature events of climate variables. Most of these studies have been conducted over Chinese and Indian regions. To the best of our knowledge, only one study, conducted by Islam et al. (2009), was carried out in Pakistan. Islam et al. study assessed future changes in extreme temperature events (for example, warm and cold spells, warm and cold nights, and warm and cold days) for only one future period (2071–2100) and under only the A2 scenario, using a regional climate model, Providing Regional Climates for Impacts Studies (PRECIS), with a resolution of 50 km. In general, the skill of the RCM depends greatly on the GCM's driving forces, such as land use data, land–sea contrast, and orography. Thus, RCMs are likely to inherit systematic errors present in GCMs. Moreover, RCMs are computationally intensive and dependent upon the resolution used and the domain size adopted, which limits the number of experiments for climate change scenarios (Wilby and Wigley, 1997; Hay and Clark, 2003; Fowler et al., 2007). In Islam et al.'s study, the model was validated with Climate Research Unit (CRU) and observed data. During the validation with CRU data, the researchers validated only mean monthly temperature instead of all the temperature indices which were used in their study. The model's performance was reasonably good only in February, July, August, and September, while in the other months, the researchers stated that the model showed cold and warm biases of about 2–5 °C. During validation with observed data, although more than a hundred climate stations are available in Pakistan, they used only 17 climate stations for the entire area (796,095 km^2) of the country, a number that appears to be quite insufficient. They also reported that the simulated daily data was not reliably compatible with observed data because in the model, topographic features like narrow peaks and valleys were smoothed out. In other words, to the best of our knowledge, no studies have been published so far that explore the extreme temperature events in the trans-boundary region (located in Pakistan and India) of the Jhelum River basin. While it is true that Islam et al. (2009) did cover some area of the Jhelum River basin, they restricted themselves to only the western part of the basin, which is located in Pakistan.

The present study is targeted to offer comprehensive simulations of extreme temperature events under two scenarios of HadCM3, A2 and B2, using SDSM in the trans-boundary area of the Jhelum River basin for three future periods: 2011–2040, 2041–2070, and 2071–2099. A total of 12 indices (8 intensity and 4 frequency) were used to explore temperature extremes in the basin. In addition, this study also faced the big challenge of applying SDSM to examine extreme temperature events in the Jhelum basin, which is mountainous in nature and is greatly influenced by the monsoon.

2. Study area and data description

2.1. Study area

The Jhelum River basin (JRB) is located in the north of Pakistan, and is spread between 33–35°N and 73–75.62°E, as shown in Fig. 1. The Jhelum River is one of the major tributaries of the Indus River, the largest river of Pakistan. The Indus River's drainage area is 1,165,500 km^2. The Jhelum River drains a total area of 33,342 km^2, with an elevation ranging between 235 and 6285 m. The JRB is actually the watershed of the Mangla Reservoir, the second biggest reservoir in Pakistan. The primary function of this reservoir is to supply water for irrigation. Hydropower is a byproduct of irrigation. The installed capacity of the Mangla power plant is 1000 MW, which is 6% of the country's total installed capacity. The Mangla reservoir has the capacity to irrigate 6 million hectares of land (Archer and Fowler, 2008; Mahmood and Babel, 2013).

The basin has great spatial and temporal variability in climate, with a mean annual temperature of 13.72 °C and a mean annual precipitation of 1202 mm. The northern areas of the basin are much colder than the southern areas. For example, Naran (located in the northern part of the basin) and Jhelum (located in the southern part of the basin) are the coldest and hottest climate stations in the basin, with mean annual temperatures of 6.14 °C and 23.53 °C respectively. January with a mean annual temperature of 2.9 °C and July with a mean annual temperature of 23 °C are the coldest and the hottest months respectively. Murree receives the highest precipitation among all the climate stations. Its mean annual precipitation is 1765 mm, and Srinagar, with mean annual precipitation of 764 mm, gets the lowest precipitation among all the climate stations (Mahmood and Babel, 2013).

2.2. Data description

The historical daily and monthly data of maximum temperature (Tmax) and minimum temperature (Tmin) for 14 climate stations (Fig. 1) was obtained from the Pakistan Meteorological Department (PMD), the Water and Power Development Authority of Pakistan (WAPDA), and the India Meteorological Department (IMD), for the period of 1961–2000. The data of 4 weather stations, namely Srinagar, Kupwara, Gulmarg, and Qazigund, were obtained from the IMD. The data of another 4 stations, Rawlakot, Plandri, Kotli, and Naran, were obtained from the WAPDA, and the data of

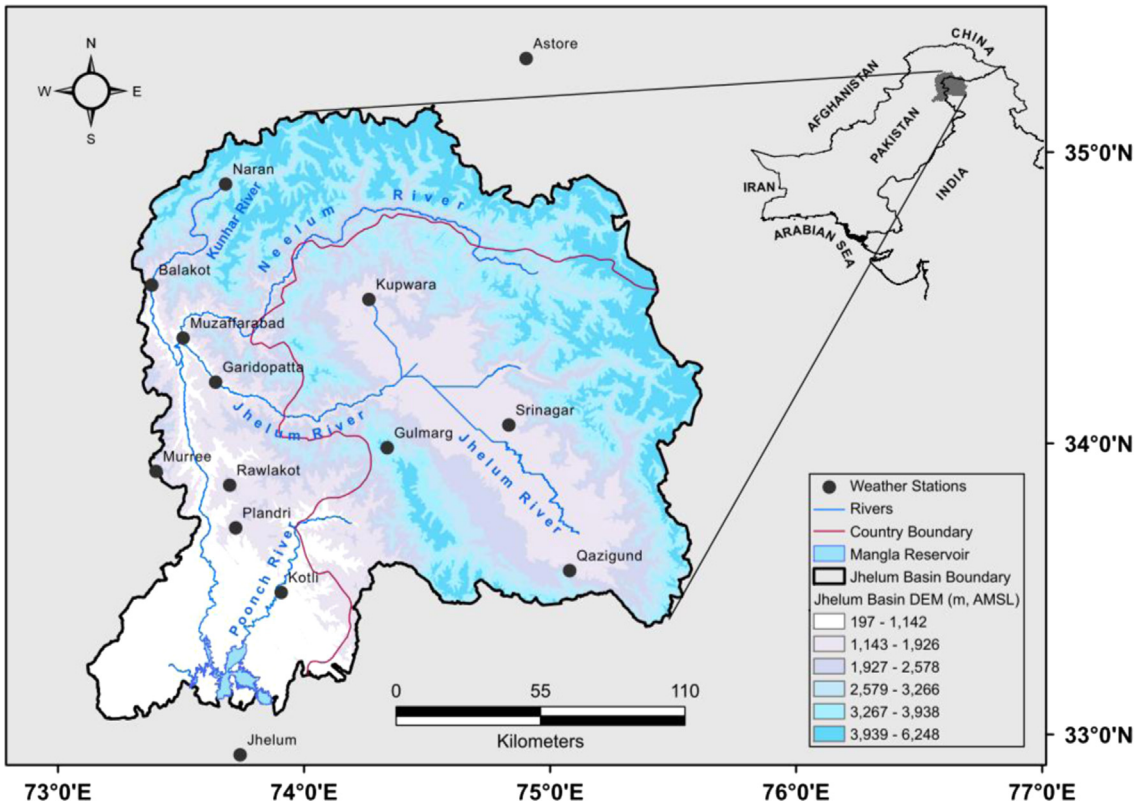

Fig. 1. Location map of the Jhelum River basin and the meteorological stations used in the present study.

the rest of the weather stations (Muzaffarabad, Jhelum, Garidopatta, Balakot, Murree, and Astore) were obtained from the PMD. From among this data of climate stations, there were some parts that were missing; such missing parts were completed with multilevel regression using WinMice software (Jacobusse, 2005).

Two types of daily predictors' data required for this study were obtained from a Canadian website (http://www.cics.uvic.ca/scenarios/sdsm/select.cgi): (a) the 26 predictors of the National Center of Environmental Prediction (NCEP) for the period of 1961–2000; and (b) the 26 predictors of HadCM3, for A2 and B2 scenarios, for the period of 1961–2099. These datasets were specially processed for SDSM. During the preparation, the NCEP predictors ($2.5^\circ \times 2.5^\circ$) were first interpolated to the grid resolution of HadCM3 ($2.5^\circ \times 3.75^\circ$) to eliminate the spatial mismatch. Then, the NCEP and HadCM3 predictors were normalized with the mean and standard deviation obtained by the long period of 1961–1990 (CCCSN, 2012).

3. Methodology

3.1. Description of SDSM

The Statistical Downscaling Model (SDSM), developed by Wilby et al. (2002), is a combination of Multiple Linear Regression (MLR) and the Stochastic Weather Generator (SWG). MLR generates statistical/empirical relationships between NCEP predictors and predictands during the screening process of predictors, and the calibration process of SDSM results in some regression parameters. These parameters, along with NCEP and GCM predictors, are used to generate a maximum of 100 daily time series to fit closely with the observed data during validation, and twenty time series are considered as the standard, a precedent set by other studies as well (Wilby et al., 2002; Gagnon et al., 2005; Chu et al., 2010).

In SDSM, various indicators—partial correlation, correlation matrix, explained variance, *P*-value, histograms, and scatter plots—can be used to select some suitable predictors from a multitude of atmospheric predictors. Multiple co-linearity, which can misguide end results among predictors, must be considered during the selection of predictors. Ordinary Least Squares (OLS) and Dual Simplex (DS) are two kinds of optimization methods available for SDSM. OLS is faster than DS and produces comparable results with DS (Huang et al., 2011). There are two kinds of sub-models, unconditional and conditional, which are used according to the requirement of the predictands. For example, the unconditional sub-model is used for an independent variable like temperature, and the conditional is used for a conditional (dependent) variable like precipitation (Wilby et al., 2002; Ashiq et al., 2010). SDSM has the ability to transform the data into different forms such as the logarithmic, square root, and fourth root to make it normal before the said data can be used in regression equations (Khan et al., 2006). To develop SDSM, two kinds of daily time series are needed: NCEP predictor daily time series and observed daily time series (Huang et al., 2011). The mathematical details of this model are provided in the study by Wilby et al. (1999).

3.1.1. The screening of predictors

The screening of large scale variables is the most important process in all types of statistical downscaling (Wilby et al., 2002; Huang et al., 2011). There are many indicators that can be used in this process. In the current study, a combination of the correlation matrix, partial correlation, and *P*-value was used. The same combination was also used in Huang et al. (2011) and Mahmood and Babel (2013). The selection of the first and the most appropriate predictor is relatively easy, but the selection of the second, third, fourth and so on is much more subjective. Therefore, a more quantitative procedure, also used by Mahmood and Babel (2013),

was applied for screening the predictors for each local climate variable and at each climate station in this study.

First, a correlation matrix between each predictand and the NCEP predictors (26 in this study) is found out; and then highly correlating predictors (10 in this case) are selected and arranged in descending order. These predictors must show a physical relation with the predictands. In this method, the highest ranked predictor is called the super predictor (SP). Following this, each predictand, along with the SP, is regressed with the remaining predictors (9 in this study) to find out the absolute correlation coefficient between the predictor and predictand, the absolute correlation coefficient between individual predictors, absolute partial correlation, and the *P*-value. Then, the predictors with *P*-value greater than α (0.05) are eliminated to make the results more statistically significant, and the predictors with high individual correlation (0.5 in this study) are also removed in order to eliminate any multi-co-linearity. According to Pallant (2007), a correlation coefficient less than 0.7 between two predictors is acceptable (Pallant, 2007). After this, percentage reduction (*PR*) in absolute partial correlation is calculated by the absolute correlation coefficient between a predictor and a predictand (*R*) and the partial correlation coefficient between a predictor and a predictand (*Pr*) using the following equation:

$$PR = \left(\frac{Pr - R}{R}\right) \quad (1)$$

At the end, the predictor with the least *PR* is selected as the second most suitable predictor. Similarly, the third, the fourth and further predictors are chosen by repeating the procedure outlined above.

It can be seen in different studies (Wilby et al., 2002; Chu et al., 2010; Mahmood and Babel, 2013) that mostly 1–3 large scale variables are believed to be enough to capture the variation of a predictand during calibration. It is better to use a smaller number of predictors during calibration because as the number of predictors increases in the regression equation, the chances of multiple co-linearity also increase. So, the fewer the predictors, the lower is the chance of multiple co-linearity during calibration.

3.1.2. Calibration and validation

Based on the available observed data, two daily datasets, 1961–1990 and 1970–1990, were selected for the calibration of Tmax and Tmin. In the present study, SDSM, using a monthly sub-model, was developed with the NCEP predictors that were selected during the screening process at each site in the Jhelum basin. Explained Variance (*E*) and Standard Error (SE) were used as performance indicators during the calibration of SDSM, a procedure also followed in studies like Chu et al. (2010), Huang et al. (2011) and Mahmood and Babel (2013).

With the calibrated model, 20 ensembles each for Tmax and Tmin were simulated for 1961–2000, feeding the NCEP, A2, and B2 predictors. The mean values of these ensembles were used in this study. The model was validated with observed data for 1991–2000 (Wang et al., 2012), using daily, monthly and seasonal time series (Huang et al., 2011). In the present study, three performance indicators—the coefficient of determination (R^2), the ratio of simulated to observed standard deviations (RS), and the root mean square error (RMSE)—were used for validation (Wang et al., 2012). RS indicates the degree of dispersion and should be closer to 1. A value of 1 shows that both datasets—observed and simulated—have the same kind of dispersion. R^2 and RMSE describe the accuracy of the model. For this study, these indicators were calculated for each climate station, and then the mean values of each indicator were obtained from all the stations. In addition, the mean monthly, seasonal and annual values of extreme indicators calculated from simulated Tmax and Tmin daily time series (NCEP,

Table 2
Selected predictors for Tmax and Tmin during screening, for calibration, in the Jhelum River basin.

Predictor name	Code	Abs. Pr.	Relationship b/w predictand (Tmax) and predictors
Tmin (predictand)			
Mean temperature at 2 m height	temp	0.76	These predictors show physical and logical relationships with the predictand (Tmax). Mean temperature at 2 m height (temp) is directly proportional with the Tmax, and others predictors are indirectly proportional to Tmax
Surface zonal velocity	p_u	0.38	
Surface vorticity	p_z	0.32	
850 hPa vorticity	P8_z	0.25	
500 hPa relative humidity	r500	0.22	
Tmin (predictand)			
Mean temperature at 2 m height	temp	0.82	Same as Tmax
Surface zonal velocity	p_u	0.37	
850 hPa vorticity	P8_z	0.32	
Surface vorticity	p_z	0.32	
Surface relative humidity	rhum	0.18	
500 hPa relative humidity	r500	0.12	

Abs. Pr.: absolute partial correlation coefficient.

Table 1
Description of extreme temperature indices used in this study.

Code	Description	Definition	Units
Intensity indices			
TXx	Hottest days	Max values of daily max temperature	°C
TNx	Hottest nights	Max values of daily min temperature	°C
TXn	Coldest days	Min values of daily max temperature	°C
TNn	Coldest nights	Min values of daily min temperature	°C
TX_90P	Hot days	90th percentile value of data describes that at least 90% of the values in the data are less than or equal to this value	°C
TN_90P	Hot nights	90th percentile value of data describes that at least 90% of the values in the data are less than or equal to this value	°C
TX_5M	Max_5Tot	Max 5 day average of Tmax	°C
TN_5M	Max_5M	Max 5 day average of Tmin	°C
Frequency indices with fixed thresholds			
HD	Hot days	Number of days with Tmax > 35°C	days
CD	Cold days	Number of days with Tmax < 15°C	days
HN	Hot nights	Number of days with Tmax > 20°C	days
FD	Frost days (Cold nights)	Number of days with Tmax < 0°C	days

Table 3
Performance assessment of SDSM during validation (1991–2000) for Tmax (Tmin), in the Jhelum River basin.

NCEP	R^2 Tmax (Tmin)	RMSE (°C) Tmax (Tmin)	RS Tmax (Tmin)
Daily	0.77 (0.86)	3.49 (2.65)	0.88 (0.92)
Monthly	0.93 (0.95)	1.87 (1.47)	0.96 (0.96)
Seasonal	0.95 (0.97)	1.39 (1.07)	0.98 (0.98)
A2			
Monthly	0.92 (0.94)	2.10 (1.74)	0.98 (0.96)
Seasonal	0.95 (0.96)	1.46 (1.19)	1.00 (0.97)
B2			
Monthly	0.92 (0.93)	2.15 (1.82)	0.98 (0.96)
Seasonal	0.95 (0.96)	1.56 (1.28)	1.00 (0.98)

RS—Ratio of standard deviation of simulated data to observed data.

A2, and B2) were plotted against the observed datasets. This method has been used by many users of SDSM (for instance, Ashiq et al., 2010; Chu et al., 2010; Wang et al., 2012) in order to observe the variations and patterns.

3.2. Future changes in extreme temperature indices

After successful validation, the daily time series of Tmax and Tmin were generated for three future periods—the 2020s (2011–2040), the 2050s (2041–2070) and the 2080s (2071–2099)—feeding the predictors of A2 and B2. In this study, in order to get realistic results, bias correction (BC)—discussed in detail below—was applied to these datasets to remove any biases in the simulated data. For this, more recent datasets for the period of 1980–2009 were applied to calculate mean monthly biases using observed and simulated (A2 and B2) temperatures (Tmax and Tmin). Mahmood and Babel (2013) concluded that recent datasets give better results than earlier datasets in the application of BC. In this study, these biases were adjusted with the daily time series of three future periods, according to their respective months. At the end, the changes in all extreme indicators for the three future periods were calculated by comparing them to the baseline period. In this study, the period from 1961 to 1990 was taken as the baseline period because this period has been used in the majority of climate change studies across the world (Huang et al., 2011). A 30-year period is also considered long enough to define the local climate because such a lengthy period is likely to include dry, wet, cool, and warm periods. The IPCC also recommends such a length (of 30 years) for the baseline period (Gebremeskel et al., 2005).

3.3. Bias correction

Bias correction (BC) has been used in several studies, such as Salzmann et al. (2007) and Mahmood and Babel (2013), to remove biases from the daily temperature series of downscaled data. In this technique, first, the biases are calculated by subtracting the mean monthly (30 years) observed data from the mean monthly simulated control data. Then, the biases are adjusted with future simulated daily time series, according to their respective months. More details about this method are given in Salzmann et al. (2007). The following equation is used to correct the biases of temperature daily time series:

$$T_d = T_S - (\overline{T_C} - \overline{T_o}) \quad (2)$$

T_d—the de-biased (corrected) daily temperature data for the future periods (e.g., 2011–2040 and 2041–2070).
T_S—the daily temperature data generated by SDSM for the future period (e.g., 2011–2040 and 2041–2070).
$\overline{T_C}$ —the long-term mean monthly values of simulated temperature for the control period (e.g. 1980–2009).
$\overline{T_o}$—the long-term mean monthly values of observed temperature for the control period (e.g. 1980–2009).

3.4. Extreme temperature indices

One of the main concerns while assessing extreme climate events is properly defining extreme indices for climate variables (temperature and precipitation). Different studies have defined varying indices according to their study regions' climates. While these indices may have similar names, their definitions and their ways of calculations can be significantly different (Zhang et al., 2011). Recently, the Expert Team on Climate Change Detection Indices (ETCCDI) has developed a core set of 27 indices to analyze the wide range of extreme climate changes. In the current study, 12 temperature indices (Table 1) out of the ETCCDI's recommendations were used to explore possible changes in temperature extremes in the future in the trans-boundary region of the Jhelum River basin. The same kinds of indices were also used to assess the changes in extreme temperature events in India (Revadekar et al., 2012) and Pakistan (Islam et al., 2009).

4. Results and discussion

4.1. Screening of predictors

Table 2 illustrates the selected predictors with mean absolute partial correlation (P.r) for Tmax and Tmin with a confidence level of 95%. During the screening process, the *temp* predictor was seen as the super predictor for both Tmax and Tmin, in the basin. These selected predictors (Table 2) also showed physical relationships with the local variables (Tmax and Tmin). The same kinds of predictors have been used in and around the Jhelum River basin in studies like Chu et al. (2010), Huang et al. (2011), and Mahmood and Babel (2013). For each site, different combinations of predictors in the presence of the super predictor were used for each predictand to improve the performance of SDSM during calibration.

4.2. Calibration and validation

4.2.1. Calibration

During the calibration of SDSM using NCEP predictors, two indicators—Explained Variance and Standard Error—were used to check the model's performance. The mean explained variances, calculated from different sites, range between 60–72% and 67–85% for Tmax and Tmin respectively, and the mean standard error lies between 1 and 2.5 °C for both the variables. The results arrived at are satisfactory and comparable to some previous studies conducted in and around the Jhelum River basin, such as Wilby et al. (2002), Huang et al. (2011), Souvignet and Heinrich (2011) and Mahmood and Babel (2013).

4.2.2. Tabular validation

During the validation process, daily data for Tmax and Tmin was generated (using NCEP, A2 and B2 predictors) for the period of 1991–2000 and compared with observed data by calculating R^2, RMSE and RS (Table 3). These indicators were calculated from the daily, monthly and seasonal time series of NCEP, and from the monthly and seasonal time series of A2 and B2. R^2 and RMSE calculated from NCEP are better than the values obtained under A2 and B2 except RS under A2, because the model was calibrated with NCEP predictors. However, the indicators calculated from the daily time series of NCEP show lower performance than the monthly

and seasonal time series of NCEP, A2 and B2. Nonetheless, these results of validation are also comparable with previous studies carried out in and around the Jhelum River basin (Ashiq et al., 2010; Wang et al., 2012; Mahmood and Babel, 2013).

4.2.3. Graphical validation before bias correction

Fig. 2 shows a graphical comparison of simulated mean monthly, seasonal and annual extreme intensity indices of temperature with observed data. The figure also examines the patterns and variations captured by the model. It can be seen clearly that all intensity indices are well overestimated by SDSM except TXn and TNn, where the model underestimates.

Fig. 3 shows comparison of frequency extreme indicators of temperature for performance assessment of SDSM in the process of validation. It is observed that Hot days (HDs) are overestimated in May–June and underestimated in July–September, and hot nights (HNs) are well overestimated in June–September. SDSM overvalues cold days (CDs) in December–February and undervalues in other months. On the other hands, the model well underestimates cold nights (FDs) in all months.

4.2.4. Graphical validation after bias correction

As the intensity and frequency indicators simulated by SDSM were not satisfactory, the bias correction method was applied to minimize the biases between simulated and observed data. Fig. 4 shows a graphical comparison of simulated mean monthly, seasonal and annual extreme intensity indices of temperature with observed data. The figure also examines the patterns and variations captured by the model. It can be seen clearly that all intensity indices are well simulated by SDSM. In this study, the hottest days (TXx) were slightly underestimated in March and in winter (December–January–February) and slightly overestimated in August, September and October as well as in autumn (September–October–November). The temperatures in the hottest nights

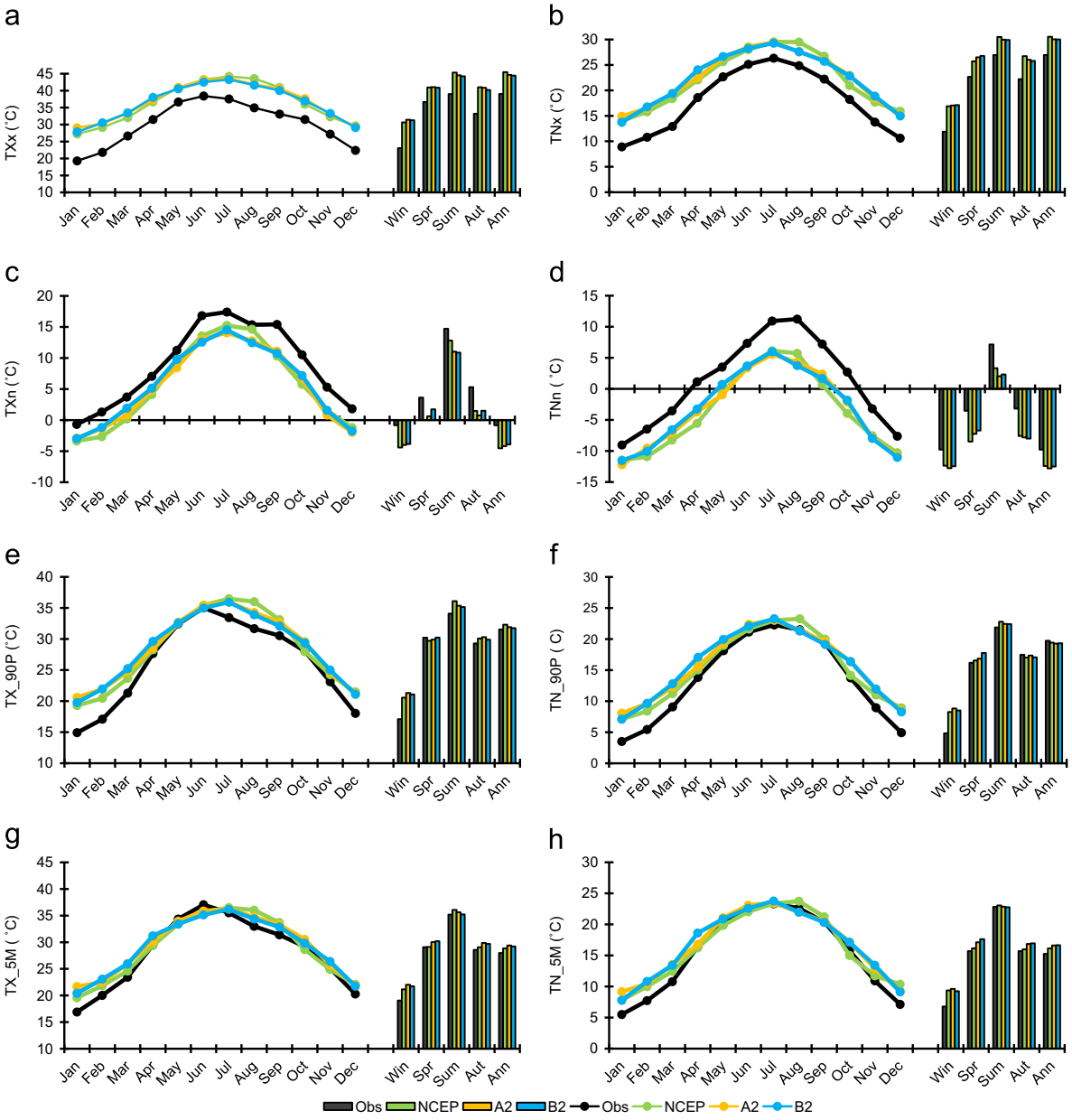

Fig. 2. Comparison of intensity extreme indices of temperature for validation in the Jhelum basin, before application of bias correction: (a) TXx, (b) TNx, (c) TXn, (d) TNn, (e) TX_90P, (f) TN_90P, (g) TX_5M and (h) TN_5M.

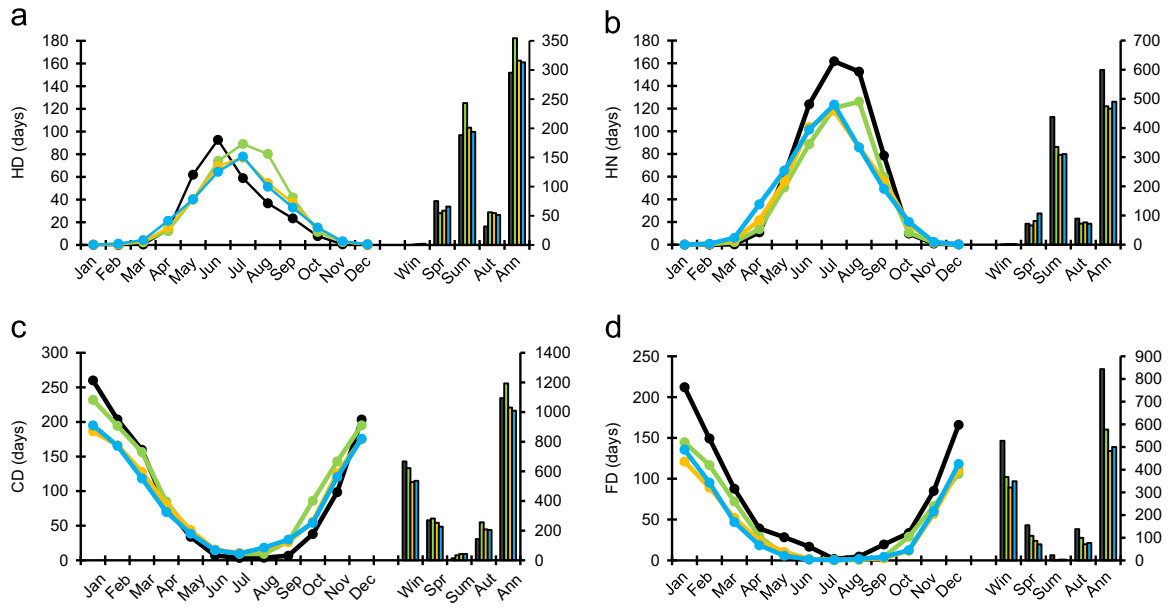

Fig. 3. Comparison of frequency extreme indices of temperature for validation in the Jhelum basin, before application of bias correction (a) HD, (b) HN, (c) CD and (d) FD.

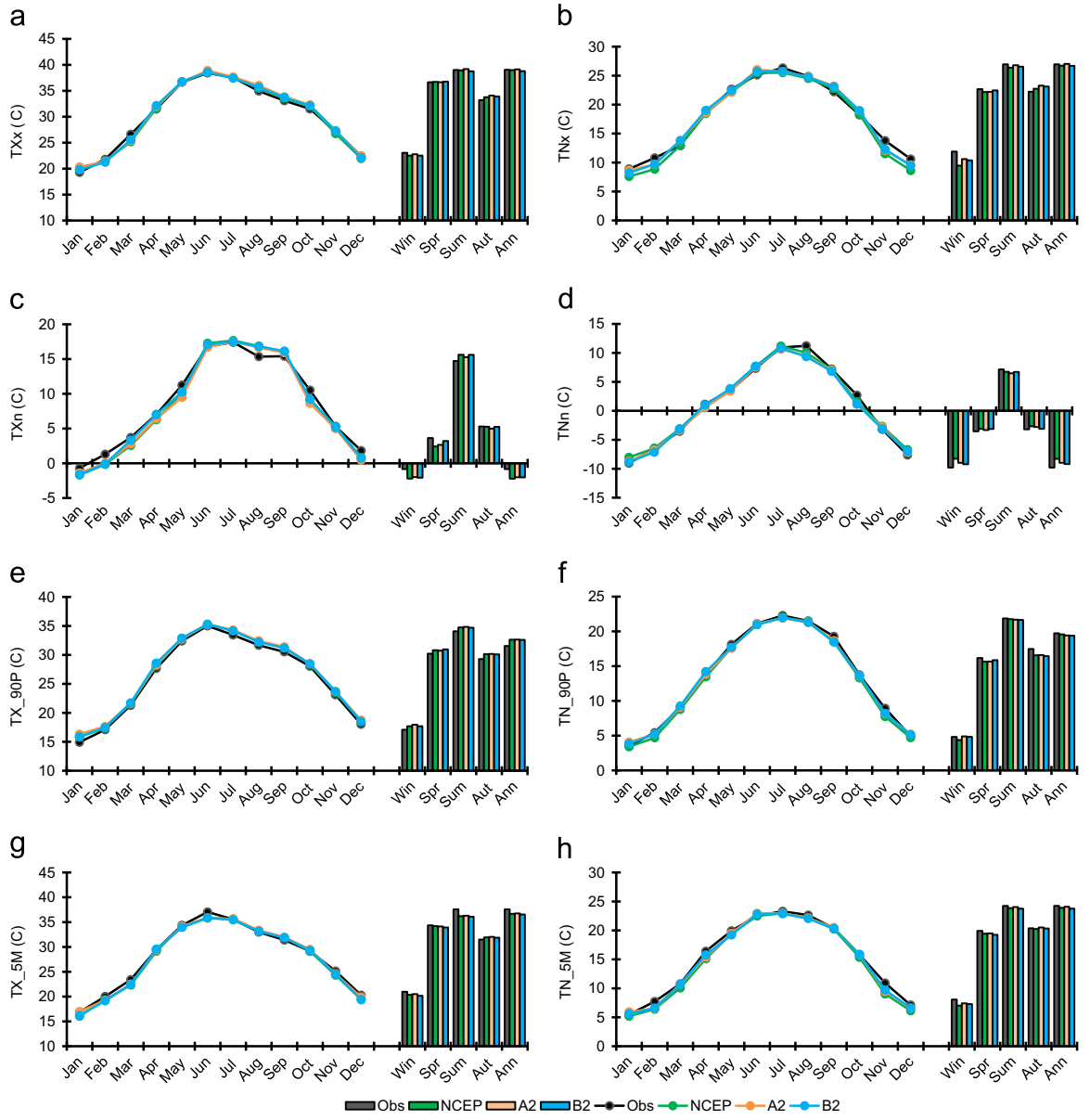

Fig. 4. Comparison of intensity extreme indices of temperature for validation in the Jhelum basin, after application of bias correction: (a) TXx, (b) TNx, (c) TXn, (d) TNn, (e) TX_90P, (f) TN_90P, (g) TX_5M and (h) TN_5M.

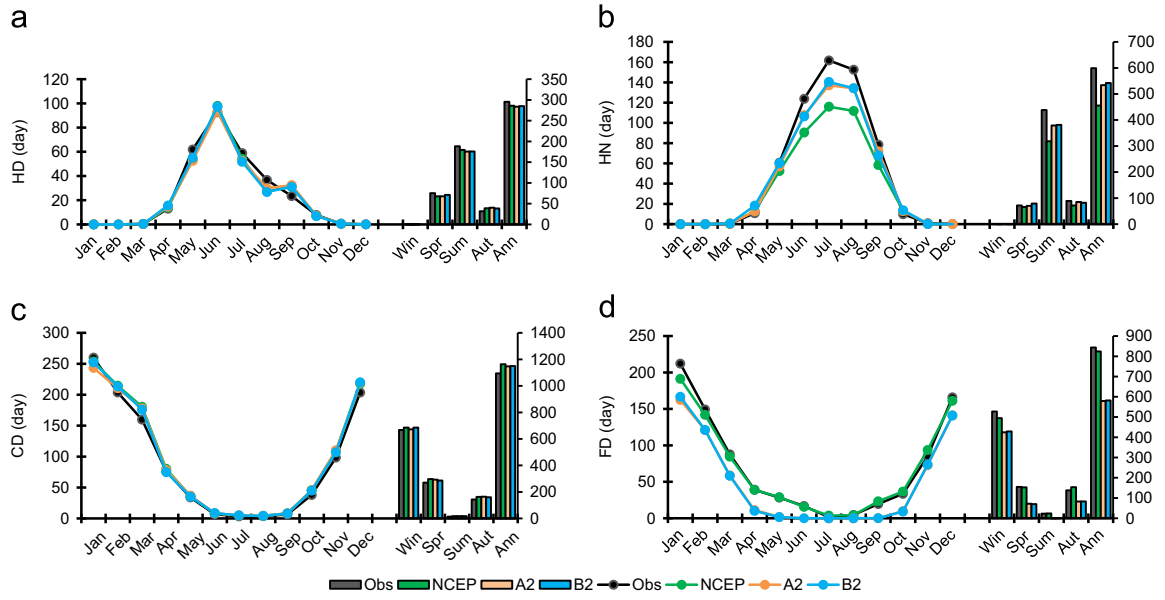

Fig. 5. Comparison of frequency extreme indices of temperature for validation in the Jhelum basin, after application of bias correction: (a) HD, (b) HN, (c) CD and (d) FD.

(TNx) were marginally underestimated in the months of July, November, December, January, and February and in all seasons except in winter. SDSM overestimated the coldest days (TXn) in winter and spring (March–April–May) and underestimated them in summer (June–July–August). The simulated temperature of the coldest nights (TNn) was lower in July. The model gave lower and higher values in hot day temperature (TX_90P) and hot night temperature (TN_90P), respectively, in all the seasons. Max five days mean temperatures (TX_5M and TX_5M) were also underestimated by the model in all the seasons.

Fig. 5 shows a graphical comparison of frequency extreme indicators of temperature for performance assessment of SDSM in the process of validation. These indicators were not as well simulated by the model as intensity indicators were. Hot days (HDs) and cold days (CDs) are relatively better simulated than hot nights (HNs) and cold nights (FDs). HDs were slightly underestimated in spring and summer but overestimated in autumn, and CDs were overestimated in all the seasons, even in the annual time frame. HN and FD were slightly underestimated in all the seasons but greater differences were seen in summer (HN) and winter (FD).

On the whole, during validation, the present study showed much better results than Islam et al. (2009) (a study conducted over Pakistan using RCM) and gave comparable results with studies like Wang et al. (2012) (conducted in the Yellow River basin of China using SDSM) and Revadekar et al. (2012) (conducted in India using RCM). The indices calculated from downscaled data from NCEP predictors were slightly better than A2 and B2. However, the results of A2 and B2 were comparable with NCEP, which proves the applicability of SDSM in the study area for the future.

4.3. Future changes in extreme temperature events

Two time series, Tmax and Tmin, were produced by SDSM for the 2020s, 2050s and 2080s under A2 and B2. Then, 8 intensity and 4 frequency extreme indices were calculated from this data and compared with the baseline period (1961–1990) to analyze the changes in these three future periods in the Jhelum River basin (Tables 4 and 5).

4.3.1. Intensity temperature extremes

The seasonal and annual future changes in intensity indices are described in Table 4. The hottest days (TXx) and hottest nights (TNx) are projected to be warmer in almost all the seasons except in winter (TNx) and in all three future periods. The maximum increase in the hottest days can be observed in winter, with 3.96 °C in the 2080s under A2. In contrast, the maximum decrease in the coldest nights can be observed in winter, with 4.12 °C in the 2080s under A2. However, both indices show an annual increase in temperature in all three future periods except in the 2020s under B2. According to the predictions, the coldest days (TXn) are likely to be severe (much cold) in almost all seasons except winter, with a maximum decrease of 3.72 °C in autumn under B2 in the 2020s. By contrast, the temperature of the coldest nights (TNn) is projected to increase in all the seasons except in summer, with a maximum increase of 4.70 °C in winter under A2 in the 2080s.

The percentile based indices, TX_90P (hot days) and TN_90P (hot nights), are predicted to increase in intensity in all three future periods and in almost all the seasons—with maximum increases of 2.09 °C and 1.46 °C respectively in the spring season under the A2 scenario (2080s). TX_5M and TN_5M are also predicted to increase in intensity in all three future periods and in almost all the seasons except in winter (TN_5M).

It is clear that all intensity indices show positive (increase) mean annual changes except TXn (hottest nights), and these change will be more towards the end of this century. As expected, the changes under A2 are greater than under B2.

4.3.2. Frequency temperature extremes

The seasonal and annual future changes in frequency indices (for instance, the number of hot days, cold days, hot nights, and frost nights) are described in Table 5. The number of hot days (HD) and hot nights (HN) is projected to increase in almost all three future periods and in all the seasons. For example, under A2 in the 2080s, the number of hot days and hot nights will increase (annually) by 150 days (50%) and 167 days (28%) respectively. In contrast, the number of cold days (CD) and frost days (FD) will decrease in the future. For example, under A2 in the 2080s, the numbers of cold and frost days (annually) are projected to

Table 4
Future changes in intensity extreme indices of temperature with respect to the baseline period (1961–1990) in the Jhelum River basin.

Indicator	Season	1961–1990	2020s		2050s		2080s	
		Abs.	A2	B2	A2	B2	A2	B2
TXx (°C)	Win	23.1	3.11	3.14	3.87	3.43	3.96	3.76
	Spr	36.7	0.22	0.24	0.83	0.40	1.47	0.77
	Sum	39.0	0.20	−0.02	0.74	0.54	0.93	0.73
	Aut	33.2	0.54	0.81	1.17	0.82	1.24	1.07
	Ann	39.0	0.17	−0.06	0.74	0.37	1.09	0.68
TNx (°C)	Win	11.9	−3.96	−4.12	−3.18	−3.89	−3.87	−3.81
	Spr	22.7	0.11	0.00	0.64	0.19	1.01	0.45
	Sum	27.0	1.39	1.42	1.92	1.82	2.24	2.00
	Aut	22.2	0.64	0.73	1.16	0.90	1.53	0.85
	Ann	27.0	0.32	0.30	0.89	0.69	1.13	0.90
TXn (°C)	Win	−0.8	−0.05	0.00	0.33	0.30	0.56	0.69
	Spr	3.6	−1.94	−1.65	−1.53	−1.38	−0.93	−1.10
	Sum	14.7	−2.49	−2.41	−3.08	−2.27	−2.19	−2.07
	Aut	5.3	−3.61	−3.71	−3.44	−3.52	−2.63	−3.18
	Ann	−0.8	−2.11	−2.02	−1.68	−1.68	−1.44	−1.31
TNn (°C)	Win	−9.8	4.06	3.89	4.06	3.92	4.70	4.09
	Spr	−3.5	2.86	2.79	2.78	2.93	3.73	3.08
	Sum	7.1	−1.65	−1.78	−1.60	−1.28	−0.72	−1.18
	Aut	−3.2	1.94	2.02	1.90	2.49	3.07	2.50
	Ann	−9.8	4.28	4.09	4.26	4.13	4.93	4.27
TX_90P (°C)	Win	17.1	0.57	0.63	1.19	0.90	1.31	1.17
	Spr	30.2	0.76	0.81	1.42	1.08	2.09	1.46
	Sum	34.1	−0.22	−0.13	0.21	0.14	0.53	0.41
	Aut	29.3	0.15	0.27	0.47	0.44	0.83	0.59
	Ann	31.5	0.23	0.31	0.64	0.55	1.02	0.79
TN_90P (°C)	Win	4.8	−0.10	−0.10	0.49	0.04	0.37	0.23
	Spr	16.2	0.48	0.32	0.90	0.51	1.46	0.75
	Sum	21.9	0.19	0.13	0.49	0.35	0.76	0.53
	Aut	17.5	0.44	0.57	0.73	0.67	1.18	0.78
	Ann	19.7	0.19	0.14	0.46	0.31	0.76	0.48
TX_5M (°C)	Win	21.0	1.94	1.93	2.59	2.22	2.81	2.52
	Spr	34.4	0.29	0.28	1.05	0.45	1.58	0.83
	Sum	37.6	1.40	1.38	1.75	1.70	2.10	1.94
	Aut	31.5	0.02	0.14	0.38	0.33	0.68	0.42
	Ann	37.6	1.30	1.32	1.79	1.62	2.16	1.91
TN_5M (°C)	Win	8.1	−2.69	−2.72	−2.05	−2.51	−2.37	−2.35
	Spr	19.9	0.77	0.61	1.37	0.89	1.85	1.09
	Sum	24.2	1.57	1.51	1.93	1.77	2.30	2.00
	Aut	20.4	0.98	0.89	1.35	1.05	2.00	1.21
	Ann	24.2	0.32	0.23	0.79	0.48	1.05	0.74

Table 5
Future changes in frequency extreme indices of temperature with respect to the baseline period (1961–1990) in the Jhelum River basin.

Indicator	Season	1961–1990	2020s		2050s		2080s	
		Abs.	A2	B2	A2	B2	A2	B2
HD (day)	Win	0	1	1	2	1	1	1
	Spr	75	16	28	58	40	87	59
	Sum	188	−18	12	23	39	43	46
	Aut	32	−15	−3	−1	7	20	12
	Ann	295	−16	38	83	87	150	118
HN (day)	Win	0	4	4	4	4	4	4
	Spr	72	16	9	52	23	91	35
	Sum	438	−56	−66	−25	−31	9	−34
	Aut	89	23	32	35	37	63	33
	Ann	599	−13	−21	66	33	167	37
CD (day)	Win	667	−42	−62	−98	−95	−191	−188
	Spr	270	−21	−18	−50	−35	−112	−73
	Sum	14	−7	−5	−12	−10	−18	−15
	Aut	143	−60	−65	−82	−78	−121	−99
	Ann	1094	−129	−150	−241	−218	−442	−375
FD (day)	Win	528	−118	−116	−149	−139	−228	−204
	Spr	155	−3	1	−12	−6	−41	−22
	Sum	23	−1	−1	−1	−1	−1	−1
	Aut	138	−36	−39	−49	−50	−81	−62
	Ann	844	−158	−156	−212	−197	−354	−291

Abs.—Absolute values *Win*—Winter (December–January–February), *Spr*—Spring (March–April–May), *Sum*—Summer (June–July–August), *Aut*—Autumn (September–October–November).

decrease by 442 days (40%) and 354 days (42%) respectively, relative to the baseline. This decrease is much more significant in winter. These results show that the frequency of hot temperature extremes will increase and the frequency of cold temperature extremes will decrease in the future. Similar conclusions have also been presented in the Fifth Assessment Report of the IPCC for most land areas in the world (IPCC, 2013). The changes in the magnitude of extreme events are higher (the same as intensity indices) under A2 than under B2. Such a result is to be expected because A2 is a scenario that presents worse conditions (higher CO_2) than B2.

It was realized during validation that SDSM, for most of the time, underestimates all the frequency indicators except CD. Thus, the frequencies may increase more (in the case of HD and HT) and decrease more (in the case of CD) than what the results project in Table 5. The frequency of FD may increase in the 2020s (although it is shown to be decreasing in Table 5), or there will be a lesser decrease in the 2080s than what the results indicate. In other words, these biases must be considered during the decision making process of any future oriented project.

5. Conclusions

In the present study, SDSM, a widely used decision support tool, was successfully calibrated (1961–1990) and validated (1991–2000) to explore future changes in 12 extreme indices (8 intensity and 4 frequency) of temperature in the trans-boundary area of the Jhelum River basin for the future periods of 2011–2040, 2041–2070, and 2071–2099 under A2 and B2 scenarios, relative to the baseline period of 1961–1990. The followings are the main conclusions of this study.

During validation, SDSM performed much better with the results obtained from the seasonal and monthly time series than the daily time series. That is, the results were slightly better when based on the seasonal time series than the monthly time series. The performance of the model was better with NCEP data than A2 and B2. Nonetheless, the results from A2 and B2 were comparable with NCEP, which proves the applicability of SDSM in the mountainous basin when attempting to simulate extreme temperature indices for the future. SDSM performed better in the case of intensity extreme indices than frequency indices during the validation process. On the whole, the model performed reasonably well for all extreme indices.

For all three future periods and under both scenarios, almost all intensity extreme indices showed mean annual increases, except coldest days (TXn). This indicates more warming towards the end of this century. The increasing annual changes in the hottest and coldest nights related to Tmin were projected to be higher than the hottest and coldest days related to Tmax. By contrast, the changes in hot nights (TN_90P) and 5 days max mean (TN_5M) related to Tmin were predicted to be lower than hot days (TX_90P) and 5 days max mean (TX_5M) related to Tmax. The maximum positive (increasing) annual changes were observed for the coldest

nights (TNn) and the maximum negative (decreasing) changes were seen for the coldest days (TXn). So, the intensity of coldest nights will be lower in the future than it is in the present, and the intensity of the coldest days will be more than the present values. The seasonal changes in the intensity temperature indices are also projected to increase in almost all the seasons except winter (TNx and TN_5M) and summer (TNn), both of which show a definite seasonal warming in the future.

In the case of frequency indices, the number of hot days and hot nights are projected to increase, and by contrast, the frequency of cold days and cold night are predicted to decrease in all three future periods. This also shows a clear warming in the future in the Jhelum River basin. In the case of seasonal changes, all seasons show warming effects in the basin. However, these effects are more serious in spring (HD and HN) and winter (CD and FD).

On the whole, the changes in all intensity and frequency temperature indices show that warm extremes in the Jhelum basin will be more and cold extremes will be fewer in the future. Some of the preliminary results about the future changes in extreme temperature indices were explored in this study. However, much more research is needed for a clearer understanding of the future changes in the climate extremes over the complex mountainous typography in this monsoon-dominant basin. For example, ensemble projections of the most recent and high resolution GCMs and/or RCMs can be used to explore the future changes in climate extreme events and to understand the uncertainties related to these climate models.

Acknowledgments

This study is a part of the doctoral research work of the first author conducted at the Asian Institute of Technology (AIT), Thailand. The authors would like to acknowledge the Pakistan Meteorological Department, the Water and Power Development Authority, and the India Meteorological Department for providing important and valuable data for this research. In addition, we are thankful to the developers of SDSM for providing this model free of cost. We also extend our heartfelt gratitude to the Higher Education Commission (HEC) of Pakistan, AIT, APEC (Asia-Pacific Economic Cooperation) Climate Center (APCC), South Korea for extending financial support to the first author for his doctoral studies.

References

Archer, D.R., Fowler, H.J., 2008. Using meteorological data to forecast seasonal runoff on the River Jhelum, Pakistan. J. Hydrol. 361 (1-2), 10–23. http://dx.doi.org/10.1016/j.jhydrol.2008.07.017.

Ashiq, M., Zhao, C., Ni, J., Akhtar, M., 2010. GIS-based high-resolution spatial interpolation of precipitation in mountain–plain areas of Upper Pakistan for regional climate change impact studies. Theor Appl. Climatol. 99 (3), 239–253. http://dx.doi.org/10.1007/s00704-009-0140-y.

CCCSN. 2012. Statistical Downscaling Input: HadCM3 Predictors: A2 and B2 Experiments. ⟨http://www.cccsn.ec.gc.ca/?page=pred-hadcm3. 2013⟩.

Cheng, C.S., Auld, H., Li, Q., Li, G.L., 2012. Possible impacts of climate change on extreme weather events at local scale in south-central Canada. Clim. Change 112 (3–4), 963–979. http://dx.doi.org/10.1007/s10584-011-0252-0.

Chu, J., Xia, J., Xu, C.Y., Singh, V., 2010. Statistical downscaling of daily mean temperature, pan evaporation and precipitation for climate change scenarios in Haihe River, China. Theor. Appl. Climatol. 99 (1), 149–161. http://dx.doi.org/10.1007/s00704-009-0129-6.

Fowler, H.J., Blenkinsop, S., Tebaldi, C., 2007. Linking climate change modelling to impacts studies: recent advances in downscaling techniques for hydrological modelling. Int. J. Climatol. 27 (12), 1547–1578. http://dx.doi.org/10.1002/Joc.1556.

Frias, M.D., Minguez, R., Gutierrez, J.M., Mendez, F.J., 2012. Future regional projections of extreme temperatures in Europe: a nonstationary seasonal approach. Clim. Change 113 (2), 371–392. http://dx.doi.org/10.1007/s10584-011-0351-y.

Gachon P., St-Hilaire A., Ouarda T., Nguyen V., Lin C., Milton J., Chaumont D., Goldstein J., Hessami M., Nguyen T., Selva F., Nadeau M., Roy P., Parishkura D., Major N., Choux M., Bourque A. 2005. A first evaluation of the strength and weaknesses of statistical downscaling methods for simulating extremes over various regions of Eastern Canada, sub-component, Climate Change Action Fund (CCAF) (trans: Canada E). Montreal.

Gagnon, S., Singh, B., Rousselle, J., Roy, L., 2005. An application of the Statistical DownScaling Model (SDSM) to simulate climatic data for streamflow modelling in Québec. Can. Water Resour. J. 30 (4), 297–314. http://dx.doi.org/10.4296/cwrj3004297.

Gebremeskel, S., Liu, Y.B., de Smedt, F., Hoffmann, L., Pfister, L., 2005. Analysing the effect of climate changes on streamflow using statistically downscaled GCM scenarios. Int. J. River Basin Manage. 2 (4), 271–280. http://dx.doi.org/10.1080/15715124.2004.9635237.

Gu, H., Wang, G., Yu, Z., Mei, R., 2012. Assessing future climate changes and extreme indicators in east and south Asia using the RegCM4 regional climate model. Clim. Change 114 (2), 301–317. http://dx.doi.org/10.1007/s10584-012-0411-y.

Hay, L.E., Clark, M.P., 2003. Use of statistically and dynamically downscaled atmospheric model output for hydrologic simulations in three mountainous basins in the western United States. J. Hydrol. 282 (1–4), 56–75. http://dx.doi.org/10.1016/s0022-1694(03)00252-x.

Huang, J., Zhang, J., Zhang, Z., Xu, C., Wang, B., Yao, J., 2011. Estimation of future precipitation change in the Yangtze River basin by using statistical downscaling method. Stoch. Environ. Res. Risk A 25 (6), 781–792. http://dx.doi.org/10.1007/s00477-010-0441-9.

Huynen, M.M., Martens, P., Schram, D., Weijenberg, M.P., Kunst, A.E., 2001. The impact of heat waves and cold spells on mortality rates in the Dutch population. Environ. Health Perspect. 109 (5), 463–470.

IPCC, 2007. Climate Change 2007: the physical science basis. In: Solomon, S., Qin, D., Manning, M., Chen, Z., Marquis, M., Averyt, K.B., Tignor, M., Miller, H.L. (Eds.), Contribution of Working Group I to the Fourth Assessment Report of the Intergovernmental Panel on Climate Change. Cambridge University Press, Cambridge.

IPCC. 2013. Climate Change 2013: The Physical Science Basis. Contribution of Working Group I to the Fifth Assessment Report of the Intergovern-mental Panel on Climate Change Intergovernmental Panel on Climate Change Cambridge, United Kingdom and New York, USA.

Islam, S., Rehman, N., Sheikh, M., 2009. Future change in the frequency of warm and cold spells over Pakistan simulated by the PRECIS regional climate model. Clim. Change 94 (1–2), 35–45. http://dx.doi.org/10.1007/s10584-009-9557-7.

Jacobusse G. 2005. WinMICE User's manual.

Khan, M.S., Coulibaly, P., Dibike, Y., 2006. Uncertainty analysis of statistical downscaling methods. J. Hydrol. 319 (1–4), 357–382. http://dx.doi.org/10.1016/j.jhydrol.2005.06.035.

Lau, W.K.M., Kim, K.M., 2012. The 2010 Pakistan flood and russian heat wave: teleconnection of hydrometeorological extremes. J. Hydrometeorol. 13 (1), 392–403. http://dx.doi.org/10.1175/Jhm-D-11-016.1.

Mahmood, R., Babel, M., 2013. Evaluation of SDSM developed by annual and monthly sub-models for downscaling temperature and precipitation in the Jhelum basin, Pakistan and India. Theor. Appl. Climatol. 113 (1–2), 27–44. http://dx.doi.org/10.1007/s00704-012-0765-0.

Mastrandrea, M.D., Tebaldi, C., Snyder, C.W., Schneider, S.H., 2011. Current and future impacts of extreme events in California. Clim. Change, 10943–10970. http://dx.doi.org/10.1007/s10584-011-0311-6.

Pallant J. 2007. SPSS Survival Manual: A step by step guide to data analysis using the SPSS for windows.

Revadekar, J.V., Kothawale, D.R., Patwardhan, S.K., Pant, G.B., Kumar, K.R., 2012. About the observed and future changes in temperature extremes over India. Nat. Hazards 60 (3), 1133–1155. http://dx.doi.org/10.1007/s11069-011-9895-4.

Salzmann, N., Frei, C., Vidale, P.-L., Hoelzle, M., 2007. The application of Regional Climate Model output for the simulation of high-mountain permafrost scenarios. Global Planet Change 56 (1–2), 188–202. http://dx.doi.org/10.1016/j.gloplacha.2006.07.006.

Sanchez, E., Gallardo, C., Gaertner, M.A., Arribas, A., Castro, M., 2004. Future climate extreme events in the Mediterranean simulated by a regional climate model: a first approach. Glob. Planet Change 44 (1–4), 163–180. http://dx.doi.org/10.1016/j.gloplacha.2004.06.010.

Schar, C., Jendritzky, G., 2004. Climate change: hot news from summer 2003. Nature 432 (7017), http://dx.doi.org/10.1038/432559a.

Souvignet M., Heinrich J. 2011. Statistical downscaling in the arid central Andes: uncertainty analysis of multi-model simulated temperature and precipitation. 10.1007/s00704-011-0430-z.

Wang, X.Y., Yang, T., Shao, Q.X., Acharya, K., Wang, W.G., Yu, Z.B., 2012. Statistical downscaling of extremes of precipitation and temperature and construction of their future scenarios in an elevated and cold zone. Stoch. Environ. Res. Risk A 26 (3), 405–418. http://dx.doi.org/10.1007/s00477-011-0535-z.

Wilby, R.L., Dawson, C.W., Barrow, E.M., 2002. SDSM—a decision support tool for the assessment of regional climate change impacts. Environ. Model Softw. 17 (2), 145–157. http://dx.doi.org/10.1016/s1364-8152(01)00060-3.

Wilby, R.L., Hay, L.E., Leavesley, G.H., 1999. A comparison of downscaled and raw GCM output: implications for climate change scenarios in the San Juan River basin, Colorado. J. Hydrol. 225 (1–2), 67–91. http://dx.doi.org/10.1016/s0022-1694(99)00136-5.

Wilby, R.L., Wigley, T.M.L., 1997. Downscaling general circulation model output: a review of methods and limitations. Prog. Phys. Geog. 21, 530–548. http://dx.doi.org/10.1177/030913339702100403.

Xu, C.-Y., 1999. Climate change and hydrologic models: a review of existing gaps and recent research developments. Water Resour. Manag. 13 (5), 369–382. http://dx.doi.org/10.1023/a:1008190900459.
Zhang, X., Alexander, L., Hegerl, G.C., Jones, P., Tank, A.K., Peterson, T.C., Trewin, B., Zwiers, F.W., 2011. Indices for monitoring changes in extremes based on daily temperature and precipitation data. Wiley Interdiscip. Rev.: Clim. Change 2 (6), 851–870. http://dx.doi.org/10.1002/wcc.147.
Zong, Y., Chen, X., 2000. The 1998 Flood on the Yangtze, China. Nat. Hazards 22 (2), 165–184. http://dx.doi.org/10.1023/a:1008119805106.